Designing coupled-resonator optical waveguides based on high-Q tapered grating-defect resonators

Hsi-Chun Liu* **and Amnon Yariv**

Department of Electrical Engineering, California Institute of Technology, Pasadena, California 91125, USA
*hliu@caltech.edu

Abstract: We present a systematic design of coupled-resonator optical waveguides (CROWs) based on high-Q tapered grating-defect resonators. The formalism is based on coupled-mode theory where forward and backward waveguide modes are coupled by the grating. Although applied to strong gratings (periodic air holes in single-mode silicon-on-insulator waveguides), coupled-mode theory is shown to be valid, since the spatial Fourier transform of the resonant mode is engineered to minimize the coupling to radiation modes and thus the propagation loss. We demonstrate the numerical characterization of strong gratings, the design of high-Q tapered grating-defect resonators ($Q>2\times10^6$, modal volume = $0.38\cdot(\lambda/n)^3$), and the control of inter-resonator coupling for CROWs. Furthermore, we design Butterworth and Bessel filters by tailoring the numbers of holes between adjacent defects. We show with numerical simulation that Butterworth CROWs are more tolerant against fabrication disorder than CROWs with uniform coupling coefficient.

OCIS codes: (140.4780) Optical resonators; (230.4555) Coupled resonators; (230.5298) Photonic crystals; (130.7408) Wavelength filtering devices.

References and links

1. A. Yariv, Y. Xu, R. K. Lee, and A. Scherer, "Coupled-resonator optical waveguide: a proposal and analysis," Opt. Lett. **24**(11), 711–713 (1999).
2. F. N. Xia, L. Sekaric, and Y. Vlasov, "Ultracompact optical buffers on a silicon chip," Nat. Photonics **1**(1), 65–71 (2007).
3. A. Melloni, F. Morichetti, C. Ferrari, and M. Martinelli, "Continuously tunable 1 byte delay in coupled-resonator optical waveguides," Opt. Lett. **33**(20), 2389–2391 (2008).
4. F. N. Xia, M. Rooks, L. Sekaric, and Y. Vlasov, "Ultra-compact high order ring resonator filters using submicron silicon photonic wires for on-chip optical interconnects," Opt. Express **15**(19), 11934–11941 (2007).
5. A. Melloni, F. Morichetti, and M. Martinelli, "Four-wave mixing and wavelength conversion in coupled-resonator optical waveguides," J. Opt. Soc. Am. B **25**(12), C87–C97 (2008).
6. J. K. S. Poon, L. Zhu, G. A. DeRose, and A. Yariv, "Transmission and group delay of microring coupled-resonator optical waveguides," Opt. Lett. **31**(4), 456–458 (2006).
7. M. Notomi, E. Kuramochi, and T. Tanabe, "Large-scale arrays of ultrahigh-Q coupled nanocavities," Nat. Photonics **2**(12), 741–747 (2008).
8. T. J. Karle, D. H. Brown, R. Wilson, M. Steer, and T. F. Krauss, "Planar photonic crystal coupled cavity waveguides," IEEE J. Sel. Top. Quantum Electron. **8**(4), 909–918 (2002).
9. H. A. Haus and Y. Lai, "Theory of cascaded quarter wave shifted distributed feedback resonators," IEEE J. Quantum Electron. **28**(1), 205–213 (1992).
10. S. Nishikawa, S. Lan, N. Ikeda, Y. Sugimoto, H. Ishikawa, and K. Asakawa, "Optical characterization of photonic crystal delay lines based on one-dimensional coupled defects," Opt. Lett. **27**(23), 2079–2081 (2002).
11. A. Martínez, J. García, P. Sanchis, F. Cuesta-Soto, J. Blasco, and J. Martí, "Intrinsic losses of coupled-cavity waveguides in planar-photonic crystals," Opt. Lett. **32**(6), 635–637 (2007).
12. P. Velha, E. Picard, T. Charvolin, E. Hadji, J. C. Rodier, P. Lalanne, and D. Peyrade, "Ultra-high Q/V Fabry-Perot microcavity on SOI substrate," Opt. Express **15**(24), 16090–16096 (2007).
13. A. R. M. Zain, N. P. Johnson, M. Sorel, and R. M. De La Rue, "Ultra high quality factor one dimensional photonic crystal/photonic wire micro-cavities in silicon-on-insulator (SOI)," Opt. Express **16**(16), 12084–12089 (2008).

#161978 - $15.00 USD Received 7 Feb 2012; revised 30 Mar 2012; accepted 2 Apr 2012; published 6 Apr 2012

14. E. Kuramochi, H. Taniyama, T. Tanabe, K. Kawasaki, Y. G. Roh, and M. Notomi, "Ultrahigh-Q one-dimensional photonic crystal nanocavities with modulated mode-gap barriers on SiO_2 claddings and on air claddings," Opt. Express **18**(15), 15859–15869 (2010).
15. Q. M. Quan, P. B. Deotare, and M. Loncar, "Photonic crystal nanobeam cavity strongly coupled to the feeding waveguide," Appl. Phys. Lett. **96**(20), 203102 (2010).
16. Y. Akahane, T. Asano, B. S. Song, and S. Noda, "High-Q photonic nanocavity in a two-dimensional photonic crystal," Nature **425**(6961), 944–947 (2003).
17. A. Yariv and P. Yeh, *Photonics*, 6th ed. (Oxford University Press, 2007).
18. H. C. Liu and A. Yariv, "Synthesis of high-order bandpass filters based on coupled-resonator optical waveguides (CROWs)," Opt. Express **19**(18), 17653–17668 (2011).
19. J. W. Mu and W. P. Huang, "Simulation of three-dimensional waveguide discontinuities by a full-vector mode-matching method based on finite-difference schemes," Opt. Express **16**(22), 18152–18163 (2008).
20. V. Van, "Circuit-based method for synthesizing serially coupled microring filters," J. Lightwave Technol. **24**(7), 2912–2919 (2006).
21. C. Ferrari, F. Morichetti, and A. Melloni, "Disorder in coupled-resonator optical waveguides," J. Opt. Soc. Am. B **26**(4), 858–866 (2009).
22. S. Mookherjea and A. Oh, "Effect of disorder on slow light velocity in optical slow-wave structures," Opt. Lett. **32**(3), 289–291 (2007).
23. H. C. Liu, C. Santos, and A. Yariv, "Coupled-resonator optical waveguides (CROWs) based on tapered grating-defect resonators," in *CLEO* (San Jose, USA, 2012).
24. H. C. Liu, C. Santis, and A. Yariv, "Coupled-resonator optical waveguides (CROWs) based on grating resonators with modulated bandgap," in *Slow and Fast Light* (Toronto, Canada, 2011), p. SLTuB2.

1. Introduction

A coupled-resonator optical waveguide (CROW) consists of a sequence of weakly coupled resonators in which light propagates through the coupling between adjacent resonators [1]. Both the bandwidth and the group velocity are dictated solely by the inter-resonator coupling strength. Such a unique waveguiding mechanism has found applications such as optical delay lines, optical buffers, optical bandpass filters, interferometers, and nonlinear optics [2–5].

CROWs can be realized with various types of resonators, such as microrings [2–6], photonic crystal resonators [7, 8], and waveguide-grating resonators [9, 10]. CROWs based on waveguide-grating resonators are attractive for their natural implementation in waveguides. Grating structures are defined on waveguides to change the group velocity of light, requiring no additional design for the coupling between waveguides and CROWs. The building block of grating CROWs is a grating-defect resonator where an artificial defect is introduced in a waveguide grating. The defect cavity supports a mode with a resonant frequency inside the grating band gap. The modal field is centered at the defect and evanesces exponentially in the grating. A grating CROW consists of a sequence of defects where adjacent resonators couple to each other via the evanescent field in the intervening grating. The coupling strength depends on the product of the grating strength and the spacing between adjacent defects. Grating CROWs based on the approximation of weak gratings can be analyzed with coupled-mode equations where two counter-propagating modes are connected by the grating [9].

When the grating is strong, such as periodic air holes in a silicon waveguide, the length of each grating-defect resonator can be as short as a few microns. High density of resonators is important for optical buffers since the delay-bandwidth product is proportional to the number of resonators. CROWs based on such small resonators have been experimentally demonstrated in silicon waveguides [10]. However, the major limitation was the intrinsic propagation loss due to radiation [11]. Highly confined modes lead to large spatial Fourier components which are phase-matched with the lossy radiation modes. The resulting low quality factor of the resonators (Q<1000) leads to power decay time constant of approximately 1 picosecond, limiting applications such as optical delay lines. Because of the coupling to the higher-order (radiation) modes, coupled-mode equations which consider only forward and backward guided modes are no longer valid. Consequently, the design of grating resonators based on strong gratings usually relies on three-dimensional simulation of the entire structures.

In this paper, we propose to reduce the propagation loss of grating-defect CROWs by designing high-Q grating-defect resonators as the building blocks. High-Q grating resonators

#161978 - $15.00 USD Received 7 Feb 2012; revised 30 Mar 2012; accepted 2 Apr 2012; published 6 Apr 2012

have been demonstrated both theoretically and experimentally. Two major approaches are respectively based on tapering the grating near the defect [12, 13] and spatially modulating the grating (period or hole radius) without a physical defect section [14, 15]. Both approaches aim to define a smooth modal field. Gaussian field distributions are well-known functions which greatly reduce the coupling to radiation modes [15, 16]. We present a systematic design of high-Q tapered grating-defect resonators where 4 or 6 periods on each side of the defect are tapered. We start with a numerical characterization of gratings with different hole radii. For a given taper profile, we can determine the modal field based on the calculated grating strength as a function of hole radius and perform spatial Fourier transform of the mode. We determine the optimal taper profile which minimizes the coupling to radiation modes and confirm the results with numerical simulation of quality factor.

When CROWs are based on high-Q resonators, the coupling to radiation modes is negligible, so the coupled-mode equations are valid. The coupled-mode formalism which we will present in Section 2 is useful for the analysis and design of grating-defect resonators and CROWs. After showing the systematic design of high-Q tapered resonators in Section 3, we will demonstrate the control of inter-resonator coupling for CROWs in Section 4 and filter design based on tailoring the coupling coefficients along a CROW in Section 5. Filter design not only optimizes the transmission and dispersive properties of CROWs but also improves the tolerance of CROWs against fabrication disorder, as will be discussed in Section 6. Finally, it is worth mentioning that we design the resonators and CROWs to resonate at the Bragg wavelength of the grating in order to ensure that the resonant wavelength will not change with the number of holes. If the resonant wavelength is not at the Bragg wavelength, especially near the band edge, an extra phase section will be required when cascading resonators for CROWs, as will be shown in the appendix.

2. Coupled-mode formalism for grating CROWs

A Bragg grating is a periodic perturbation to a waveguide. A grating with a period Λ couples counter-propagating modes with a propagation constant β if the phase-matching condition is satisfied, i.e. $2\pi/\Lambda = 2\beta$. The coupled-mode equations relating the amplitudes of the forward mode a and the backward mode b are given by [17]

$$\begin{aligned} \frac{da}{dz} &= -i\delta a + i\kappa_g^*(z)b \\ \frac{db}{dz} &= i\delta b - i\kappa_g(z)a \end{aligned}, \qquad (1)$$

where $\delta \equiv \beta - \beta_B$ is the detuning from the Bragg condition, $\beta_B \equiv \pi/\Lambda$, and $\kappa_g(z)$ is the coupling coefficient of the grating. The absolute value and phase of $\kappa_g(z)$ represent the strength and phase of the grating respectively. $\kappa_g(z)$ is a constant for a uniform grating. If the grating strength is tapered, $|\kappa_g(z)|$ varies along the grating. For a grating structure distributed between $z = 0$ and $z = L_g$ and an input $a(0) = 1$ from $z = -\infty$, the general approach of solving the transmission and the field distribution is as follows: (i) Set the boundary condition at the output as $a(L_g) = 1$ and $b(L_g) = 0$ (no input from $z = \infty$). (ii) Propagate a and b from $z = L_g$ back to $z = 0$ analytically or numerically, using Eq. (1). (iii) Divide the resulting $a(z)$ and $b(z)$ by $a(0)$ to recover the input amplitude $a(0) = 1$.

A grating-defect resonator is formed by inserting an artificial defect section in a grating, as shown in Fig. 1(a). The defect section is a cavity where light is longitudinally confined by the

#161978 - $15.00 USD Received 7 Feb 2012; revised 30 Mar 2012; accepted 2 Apr 2012; published 6 Apr 2012

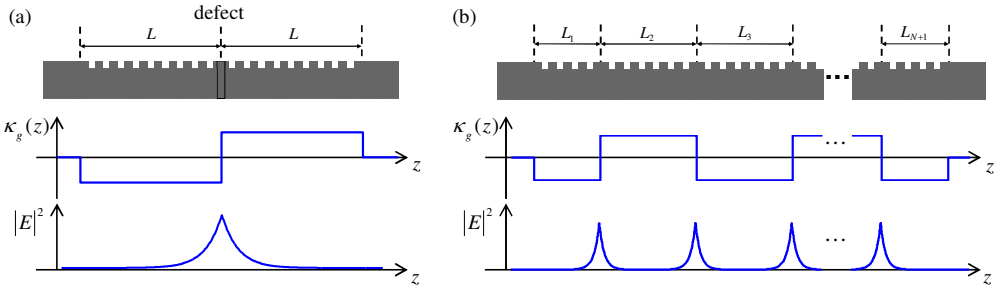

Fig. 1. Schematic drawings, coupling coefficients, and field intensity of (a) a grating-defect resonator and (b) a grating-defect CROW.

Bragg gratings at frequencies inside the band gap ($|\delta|<\kappa_g$). If the defect length is $\lambda/(4n)$ (a quarter-wave-shifted (QWS) defect; n is the effective index of the waveguide mode), the phase of $\kappa_g(z)$ is shifted by π, and the defect mode resonates at the Bragg frequency ($\delta = 0$). The distribution of the modal energy, $|a|^2 + |b|^2$, is centered at the defect and evanesces exponentially in the grating, as shown in Fig. 1(a). The modal fields (a and b) are proportional to $\exp(-\kappa_g \Delta z)$, where Δz is the distance from the defect.

A grating-defect CROW consists of a sequence of defects, where adjacent defect modes interact with each other via their evanescent fields, as shown in Fig. 1(b). $\kappa_g(z)$ alternates between κ_g and $-\kappa_g$. The inter-resonator coupling is determined by the spacing between defects, denoted as L. For a grating structure consisting of only QWS defects (i.e. a real $\kappa_g(z)$), the field distribution at $\delta = 0$ for an input $a(0) = 1$ can be derived as

$$a(z) = a(L_g)\cosh\left(\int_z^{L_g} \kappa_g(z')dz'\right) \tag{2a}$$

and

$$b(z) = -ia(L_g)\sinh\left(\int_z^{L_g} \kappa_g(z')dz'\right), \tag{2b}$$

where $a(L_g) = 1\Big/\cosh\left(\int_0^{L_g} \kappa_g(z')dz'\right)$ is the transmitted amplitude. We consider an inter-resonator spacing L and $L_1 = L_{N+1} = L/2$ at the boundary, which guarantees $\cosh\left(\int_0^{L_g} \kappa_g(z')dz'\right) = 1$ and thus unity transmission $a(L_g) = 1$. The energy stored in the grating, $E_{stored} = \int_0^{L_g} (|a|^2 + |b|^2)dz / v_g$, can be derived as $L_g\left[\sinh(\kappa_g L)/\kappa_g L\right]/v_g$, where v_g is the group velocity of the waveguide mode. Since the input power $|a(0)|^2$ is 1, the group velocity in the grating-defect CROW is given by

$$v_{g,CROW} = \frac{L_g}{E_{stored}} = v_g \cdot \frac{\kappa_g L}{\sinh(\kappa_g L)}. \tag{3}$$

The slowing factor is a function of $\kappa_g L$.

The time-domain inter-resonator coupling coefficient, denoted as κ, can be obtained by solving the frequency splitting of two coupled defect resonators separated by L, which results in

$$\kappa = \kappa_g v_g \exp(-\kappa_g L). \tag{4}$$

#161978 - $15.00 USD Received 7 Feb 2012; revised 30 Mar 2012; accepted 2 Apr 2012; published 6 Apr 2012

with the assumption of $\exp(-\kappa_g L) \ll 1$ [9, 18]. The group velocity at resonant frequency is thus $v_{g,CROW} = 2\kappa L = v_g \left[2\kappa_g L / \exp(\kappa_g L) \right]$, which, in the limit of $\exp(-\kappa_g L) \ll 1$, is the same as Eq. (3). Finally, we consider a single grating-defect resonator, as shown in Fig. 1(a). The resonator is coupled to input and output waveguides via gratings of length L. The loss rate of the mode amplitude due to coupling to each waveguide is given by $1/\tau_e = \kappa_g v_g \exp(-2\kappa_g L)$ [18]. The total loss rate is $1/\tau = 2/\tau_e$, and the quality factor of the resonator is

$$Q = \frac{1}{2}\omega\tau = \frac{\omega \cdot \exp(2\kappa_g L)}{4\kappa_g v_g}. \tag{5}$$

Q is an exponential function of L.

Figures 2(a) and 2(b) show the spectra of transmission and group delay of 10-resonator grating-defect CROWs with L = 200 μm and L = 300 μm respectively. We choose a group index of 4 and a weak grating with κ_g = 0.01/μm. The lengths of the first and last grating sections, L_1 and L_{N+1}, are chosen to be $L/2$ to match the CROW section to the waveguides [18]. According to Eq. (4), the coupling coefficients of the two CROWs differ by a factor of $\exp(\kappa_g \Delta L) = e$, which agrees with the bandwidths and the group delay shown in Fig. 2.

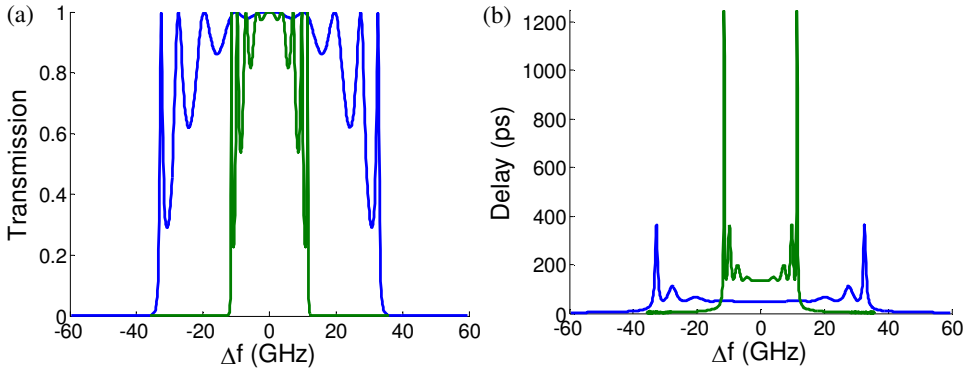

Fig. 2. Spectra of (a) transmission and (b) group delay of N = 10 grating-defect CROWs with inter-defect spacing L = 200 μm (blue) and L = 300 μm (green). κ_g = 0.01/μm.

3. High-Q tapered grating-defect resonators in silicon waveguides

3.1 Numerical characterization of Bragg gratings

Figure 3(a) shows a Bragg grating in a single-mode silicon-on-insulator waveguide which is 490 nm wide and 220 nm thick. The grating is composed of periodic air holes, which are etched through the silicon layer. For weak gratings, the evaluation of κ_g is usually based on perturbation theory – An overlap integral of the perturbation $\Delta\varepsilon(x,y)$ and the modal fields $E(x,y)$ [17]. However, this method is not accurate for strong gratings, where the modal fields are strongly perturbed. The propagation constant of the waveguide mode is also strongly perturbed by the grating. Therefore, for each hole radius r, the grating period Λ needs to be determined for a given Bragg wavelength (1570 nm throughout this paper). We design grating-defect resonators and CROWs to resonate at the Bragg wavelength for three reasons. First, the analysis based on coupled-mode equations is the simplest (δ = 0 in Eq. (1)). Second, the grating strength is maximal at the Bragg wavelength, which enables the shortest possible device length. Last, when cascading resonators for CROWs, additional waveguide sections between adjacent resonators will be required if the resonant frequency is not at the Bragg frequency (we show this in the appendix).

#161978 - $15.00 USD Received 7 Feb 2012; revised 30 Mar 2012; accepted 2 Apr 2012; published 6 Apr 2012

Given a grating with a hole radius r and a period Λ, we can determine its Bragg wavelength and κ_g by simulating the transmission and reflection of the grating. For a grating with a constant κ_g between $z = 0$ and $z = L$ and an input $a(0) = 1$, the phase of the reflected mode $b(0)$ can be derived from Eq. (1) as $\theta_r = -\pi/2 - \sin^{-1}(\delta/\kappa_g)$ if L is sufficiently long. The Bragg wavelength ($\delta = 0$) can be obtained at the condition $\theta_r = -\pi/2$. κ_g can be determined from the transmitted power at Bragg wavelength, $|a(L)|^2 = 1/\cosh^2(\kappa_g L)$.

We simulate grating structures in silicon waveguides using a 3D mode-matching method (MMM) [19]. Air holes are divided into longitudinal z-invariant sections. In each section, the total field is expressed as a superposition of the local eigen-modes (both forward and backward modes), which are solved using a finite-difference full-vectorial mode solver. Fields in adjacent sections are related by a scattering matrix which obeys continuity of the tangential components of electric and magnetic fields. The scattering matrix of the entire grating structure is obtained by cascading the scattering matrix of each section. MMMs are especially efficient for periodic structures. Once the scattering matrix of one unit cell is obtained, the entire grating structure can be constructed quickly. One major difference between our simulation and conventional MMMs is that in order to account for every component of radiation loss when simulating high-Q resonators, we use a complete set of modes. Therefore, we have to find a balance between accuracy and computation cost. This method is efficient compared to other simulation methods, especially when the grating structure is long.

Figure 3(b) shows the calculated $\kappa_g(r)$ and $\Lambda(r)$ for a Bragg wavelength of 1570 nm. Since the area of holes is proportional to r^2, $\kappa_g(r)$ is quadratic at small radii. At larger radii, $\kappa_g(r)$ becomes linear and the slope starts decreasing, since κ_g corresponds to the first-order Fourier component of the grating. On the other hand, the perturbation of the propagation constant corresponds to the constant term of the Fourier components, so $\Lambda(r)$ is nearly a quadratic curve. Note that for a hole radius of 100 nm, κ_g is 1.49/μm, which is 16% of the propagation constant and thus corresponds to a very strong grating.

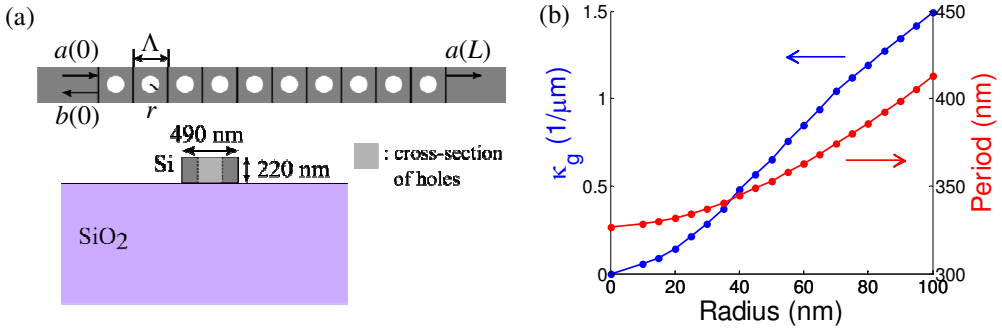

Fig. 3. (a) Schematic drawing of a strong grating in a silicon waveguide and its cross-section. (b) Simulated κ_g and grating period as functions of hole radius

3.2. Design of high-Q tapered grating-defect resonators

Grating-defect resonators in strong gratings inevitably incur radiation losses. Although the resonant mode consists of only forward and backward waveguide modes, a and b, the spatial Fourier components which are phase-matched and thus couple to the radiation modes lead to radiation loss. Figure 4(a) shows the modal field of a QWS resonator. The amplitude oscillation is due to the interference between the forward and backward modes, and the envelope decays exponentially with the distance from the defect (at $z = 0$). As a result, the spatial Fourier transform consists of two lorentzian functions which are centered at the propagation constants of the forward and backward modes, as shown in Fig. 4(b). The Fourier components whose frequencies lie within the continuum of radiation modes ($-n_{clad} < k_z/k_0 < n_{clad}$) lead to radiation

#161978 - $15.00 USD Received 7 Feb 2012; revised 30 Mar 2012; accepted 2 Apr 2012; published 6 Apr 2012

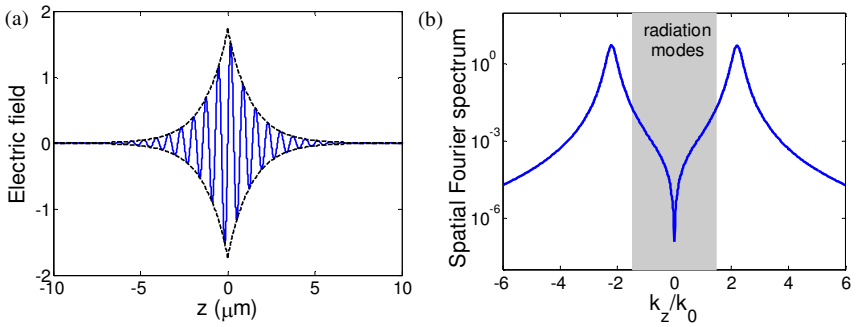

Fig. 4. (a) Field distribution of a QWS resonator mode. κ_g = 0.75/μm (b) Spatial Fourier transform of the QWS resonator mode.

loss. The loss associated with a highly localized mode is especially large, since the lorentzian functions are broad.

To reduce the radiation loss, we can engineer the modal field so as to minimize its spatial Fourier components within the radiation continuum. For example, if the envelope of the field is a Gaussian function, the Fourier transform consists of two Gaussian functions, which decay much faster than lorentzian functions. In other words, the smoother Gaussian envelope leads to narrower functions in the spatial frequency domain. The modal field is controlled by the grating strength $\kappa_g(z)$, since the envelope is proportional to $\exp\left[-\int_0^{\Delta z}\kappa_g(\Delta z')d(\Delta z')\right]$, where Δz is the distance from the defect. If Gaussian distribution is desired, $\kappa_g(\Delta z)$ should be linear.

A given profile of grating strength $\kappa_g(z)$ can be realized by the choice of the hole radii. Figure 5(a) shows a tapered grating-defect resonator where the 6 nearest unit cells on each side of the defect are tapered. Both the radii and the periods are varied to ensure the same Bragg wavelength, 1570 nm. The defect length d is chosen to be $\lambda/(4n_{eff})$ = 162.5 nm, where n_{eff} is the effective index of the waveguide mode. We choose r = 100 nm for the regular holes, which corresponds to Λ = 413 nm and κ_g = 1.49/μm according to Fig. 3(b). For the tapered grating, we assign $\kappa_{g,i} = \kappa_g[i/(n_t + 1)]^{\alpha}$ for the i-th hole, where n_t is the number of tapered holes. The radius r_i and period Λ_i of each unit cell are determined based on the curves in Fig. 3(b). $\kappa_g(z)$ is a step function which is constant within each unit cell. If α = 1, $\kappa_g(z)$ is approximately linear and leads to a Gaussian field distribution.

We consider grating-defect resonators with 4 and 6 tapered holes respectively. The objective is to find an α which minimizes the radiation loss. Figure 5(b) shows the field distribution on one side of the defect for α = 0, 0.55, and 1 based on their $\kappa_g(z)$. To estimate the radiation loss, we integrate the spatial Fourier spectrum over the radiation continuum. Figure 5(c) shows the portion of energy in the radiation continuum, η_{rad}, as a function of α for 4 and 6 tapered holes respectively. Tapering the grating reduces η_{rad} by more than 3 orders of magnitude. The effect of 6 tapered holes is better than that of 4 tapered holes. The minimum of η_{rad} occurs at α = 0.48 and 0.55 for 4 and 6 tapered holes respectively. This result shows that tapered gratings with α~0.5, corresponding to a field distribution of approximately $\exp[-(\Delta z)^{3/2}]$, are better than linear tapers with Gaussian distribution. Their field distributions are shown in Fig. 5(b), and the spatial Fourier spectra are shown in Fig. 5(d). Compared to α = 1, while the spectrum of α = 0.55 is larger at higher frequencies, it is an order of magnitude smaller within the radiation continuum. As a result, the taper profile with α = 0.55 constitutes an optimal design.

#161978 - $15.00 USD Received 7 Feb 2012; revised 30 Mar 2012; accepted 2 Apr 2012; published 6 Apr 2012

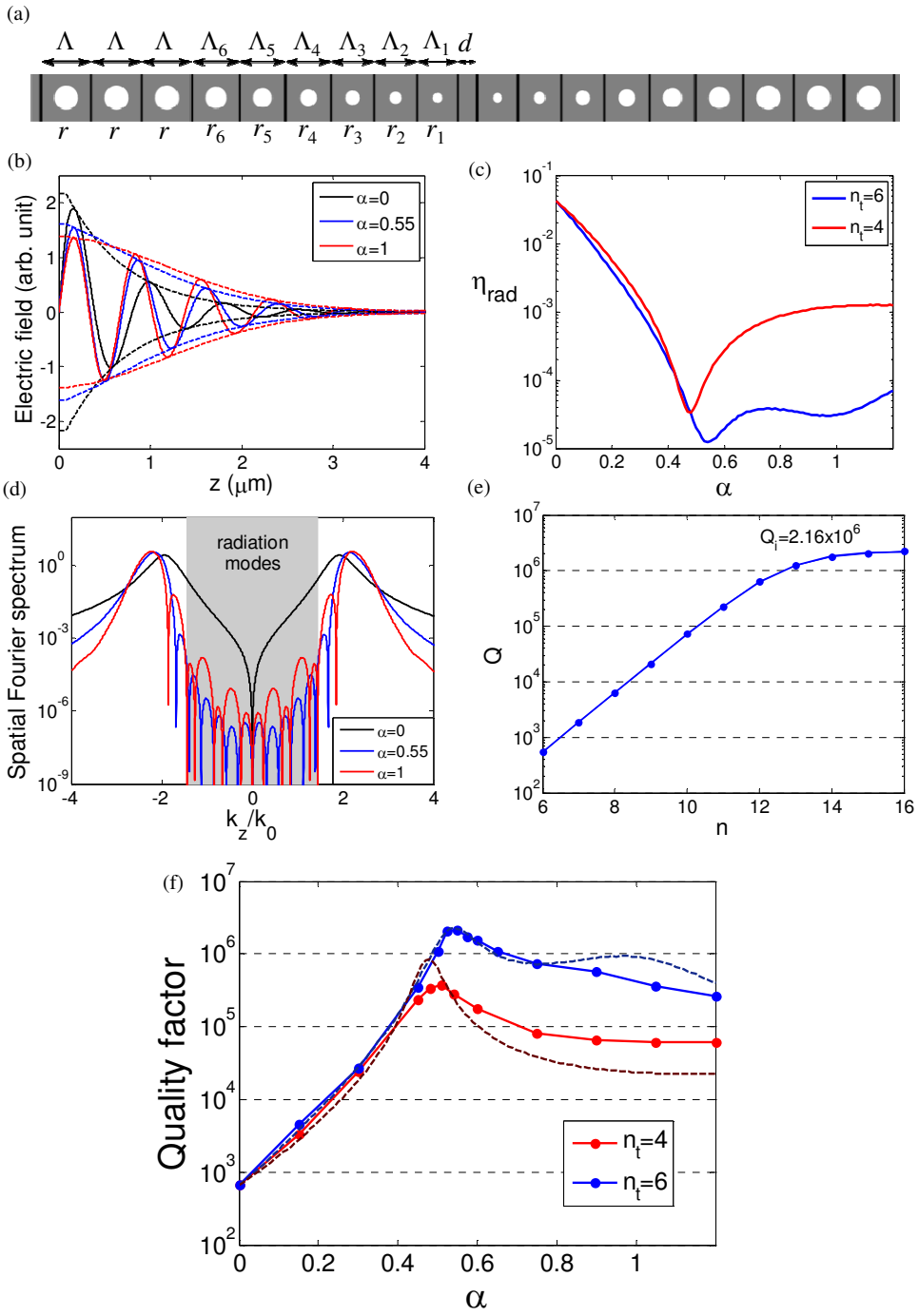

Fig. 5. (a) Schematic drawing of a tapered grating-defect resonator with 6 tapered holes. (b) Field distribution (one side of the defect) of tapered grating-defect resonators with α = 0, 0.55, and 1, respectively. (c) Energy portion in the continuum of radiation modes of grating-defect resonators as a function of α. (d) Spatial Fourier spectra of the modal fields for α = 0, 0.55, and 1. (e) Quality factor as a function of number of holes on each side of the defect. α = 0.55, n_t = 6. (f) Quality factor as a function of α. Dashed lines show η_{rad}^{-1}.

#161978 - $15.00 USD Received 7 Feb 2012; revised 30 Mar 2012; accepted 2 Apr 2012; published 6 Apr 2012

To verify the results obtained from the Fourier analysis, we simulated resonators with various α using 3D MMMs. The quality factor Q was obtained from the linewidth of resonance in the transmission spectrum. Q consists of external Q (Q_e) due to the coupling to waveguides and intrinsic Q (Q_i) due to radiation loss:

$$\frac{1}{Q} = \frac{1}{Q_e(n)} + \frac{1}{Q_i}, \tag{6}$$

where n is the number of holes on one side of the defect. In order to find Q_i, we increase n until Q is saturated at Q_i, as shown in Fig. 5(e). The quality factor as a function of α for 4 and 6 tapered holes is plotted in Fig. 5(f). We plot η_{rad}^{-1} (multiplied by a constant so that it is equal to Q at $\alpha = 0$) on the same figure for comparison. The curves of Q agree closely with η_{rad}^{-1}. The maximum of Q occurs at $\alpha = 0.51$ and 0.55 for 4 and 6 tapered holes respectively. The highest Q for 6 tapered holes is 2.16×10^6 at $\alpha = 0.55$. It is an order of magnitude higher than the theoretical Q of grating-defect resonators designed in the literature [12, 13]. The radii of the tapered holes are 41.5, 54.6, 64.8, 72.9, 82.9, 92.1 nm, and the periods are 346.3, 357.7, 367.9, 378.3, 389.7, 401.3 nm. The modal volume is $0.38\cdot(\lambda/n_{Si})^3$, which is smaller than those of 1D photonic crystal resonators resonating at frequencies near the grating band edge [14, 15]. Further increasing the number of tapered holes will result in a higher Q. However, the resulting smaller holes may not be practical.

4. CROWs based on tapered grating-defect resonators

Grating CROWs are formed by cascading the high-Q grating-defect resonators designed in Section 3. Figure 6 shows the first two resonators of a grating CROW. The inter-resonator coupling is controlled via the number of holes between neighboring defects, denoted as m. m includes the number of tapered holes ($2n_t$) and the number of regular holes (n_{reg}). In the appendix, we will show that when cascading two symmetric grating resonators with external quality factors Q_1 and Q_2 respectively, the coupling coefficient is given by

$$\kappa = \frac{\omega}{4\sqrt{Q_1 Q_2}}. \tag{7}$$

If the resonant frequency is not at the Bragg wavelength, an additional waveguide section between two resonators is required for appropriate coupling in CROWs (see appendix). We have shown in Eq. (5) that Q is proportional to $\exp(2\kappa_g L)$. For a tapered resonator, the relation is modified as

$$Q \propto \exp\left[2\int_0^L \kappa_g(z)dz\right] = \exp\left[2\sum_{i=1}^{n}\kappa_{g,i}\Lambda_i\right] = \exp\left[2\sum_{i=1}^{n_t}\kappa_{g,i}\Lambda_i\right]\cdot\exp\left[2n_{reg}\kappa_g\Lambda\right], \tag{8}$$

which breaks down into the contribution of each hole in the tapered region and the regular grating, respectively. Therefore, Q can be written as

$$Q = Q_0 \cdot a^{2n_{reg}}, \tag{9}$$

where Q_0 is the quality factor of a resonator with only the tapered region (no regular hole) and $a \equiv \exp(\kappa_g\Lambda) = 1.849$. We fit the curve in Fig. 5(e) ($\alpha = 0.55$, $n_t = 6$) with Eq. (9) and obtain $Q_0 = 548$ and $a = 1.848$. If we cascade two resonators with $n_{reg,1}$ and $n_{reg,2}$ respectively, we obtain the inter-resonator coupling coefficient given by

$$\kappa = \frac{\omega}{4\sqrt{Q_1 Q_2}} = \frac{\omega}{4Q_0} a^{-n_{reg}}, \tag{10}$$

#161978 - $15.00 USD Received 7 Feb 2012; revised 30 Mar 2012; accepted 2 Apr 2012; published 6 Apr 2012

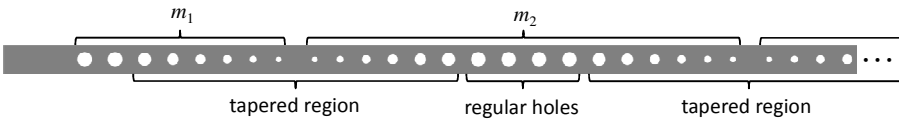

Fig. 6. Schematic drawing of the first two resonators of a grating-defect CROW.

where $n_{reg} = n_{reg,1} + n_{reg,2}$ is the total number of regular holes between two defects. For the first or last resonators, the external loss rate to the waveguides is given by (also shown in the appendix)

$$\frac{1}{\tau_e} = \frac{\omega}{4Q} = \frac{\omega}{4Q_0} a^{-2n_{reg}}, \tag{11}$$

where n_{reg} is the number of regular holes in the first or last grating section. To match between the CROW and the waveguides, we require $\kappa = 1/\tau_e$ [18]. Therefore, the number of holes in the first and last sections is one half of the number of holes in the middle sections, i.e. $m_1 = m_{N+1} = m/2$.

Figures 7(a) and 7(b) show the spectra of transmission and group delay of $N = 10$ CROWs for $m = 12$, 14, and 16 respectively ($n_{reg} = 0$, 2, and 4). The band center is at 1569.2 nm. Both the bandwidth and the group delay are dictated by m. The bandwidth is equal to 4κ and the group delay at the band center is given by $N/(2\kappa)$. Adding two holes between defects results in a factor of $a^2 = 3.415$ in κ, which agrees with simulation. Note that the maximal transmission for $m = 12$ is only 0.955. This is due to the strong index contrast between the waveguide and the grating section, which scatters light to the radiation modes. The strong index contrast can be reduced by tapering the grating at the input [13]. For larger m, the radiation loss increases due to the longer delay. The transmitted power can be written as $\exp(-\omega\tau/Q_i)$, where τ is the group delay. The delay for $m = 16$ is 106.3 ps, which leads to a transmitted power of 0.943. Including the scattering loss at the input, the transmission drops to about 0.9, which agrees with the simulation.

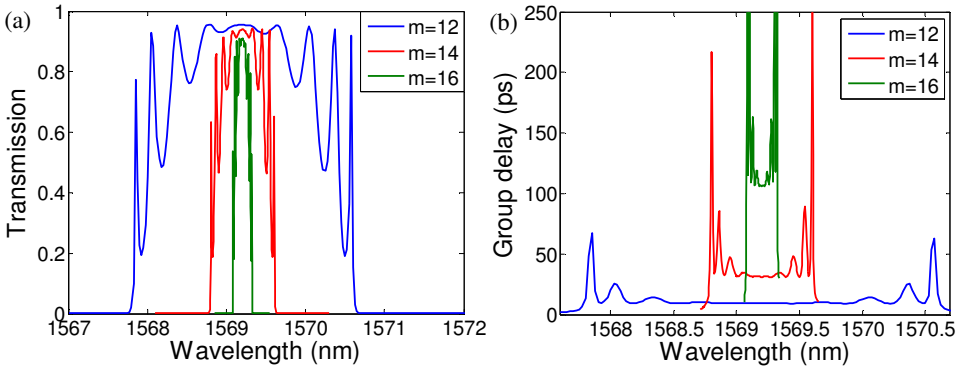

Fig. 7. Spectra of (a) transmission and (b) group delay of 10-resonator grating-defect CROWs with $m = 12$, 14, and 16 respectively.

5. Filter design based on grating CROWs

High-order bandpass filters with optimized transmission and dispersive properties can be realized in CROWs if the coupling coefficients are allowed to take on different values. For example, Butterworth filters exhibit maximally flat transmission, while Bessel filters possess maximally flat group delay. For a desired filter response, the coupling coefficients which determine the transfer function of CROWs can be derived [18, 20]. Table 1 lists the coupling

#161978 - $15.00 USD Received 7 Feb 2012; revised 30 Mar 2012; accepted 2 Apr 2012; published 6 Apr 2012

Table 1. Coupling Coefficients of $N = 10$ Butterworth and Bessel CROWs

Filter type	$(1/\tau_{e1}, \kappa_1, \kappa_2, \cdots, \kappa_{N-1}, 1/\tau_{e2}) / B$
N = 10 Butterworth	(3.196, 1.876, 0.883, 0.630, 0.533, 0.506, 0.533, 0.630, 0.883, 1.876, 3.196)
N = 10 Bessel	(3.478, 2.030, 0.932, 0.613, 0.305, 0.333, 0.652, 0.772, 1.056, 2.209, 3.745)

Table 2. Numbers of Regular Holes of $N = 10$ Butterworth and Bessel CROWs

Filter type	n_{reg}
N = 10 Butterworth	(0.495, 1.854, 3.078, 3.625, 3.896, 3.980, 3.896, 3.625, 3.078, 1.854, 0.495)
N = 10 Bessel	(0.426, 1.726, 2.990, 3.670, 4.802, 4.659, 3.568, 3.295, 2.787, 1.589, 0.366)

coefficients of $N = 10$ Butterworth and Bessel filters respectively. These coupling coefficients are normalized to a chosen bandwidth parameter B.

In grating-defect CROWs, the coupling coefficients are translated to the numbers of holes based on Eqs. (10) and (11). However, these numbers of holes are in general non-integers. Table 2 lists the numbers of regular holes corresponding to the two filters in Table 1. The bandwidth parameter B is chosen as $2\cdot\kappa(n_{reg} = 4)$ so that its bandwidth is equal to those of CROWs with uniform coupling and $n_{reg} = 4$ ($m = 16$ in Fig. 7). Since κ is an exponential function of n_{reg}, we can add an arbitrary Δn_{reg} in order to change the bandwidth without having to rederive all the n_{reg}. A non-integer n_{reg} can be realized by an integer number $n_{int} = \lceil n_{reg} \rceil$ of identical holes which are equivalent to a fraction $\gamma = n_{reg}/\lceil n_{reg} \rceil$ of a regular hole. For example, 3.6 regular holes are equivalent to 4 × 0.9 holes. This can be seen in

$$a^{n_{reg}} = \exp\left[n_{reg}\kappa_g \Lambda\right] = \exp\left[n_{\text{int}}\kappa_g(r)\Lambda(r)\right]. \tag{12}$$

Therefore, we need to determine the hole radius r whose $\kappa_g(r)\Lambda(r)$ is equal to $\gamma\kappa_g\Lambda$. This can be done by interpolating the curve of $\kappa_g\Lambda$ versus r. For example, the radius of a $\gamma = 0.9$ hole is 90.1 nm. If n_{reg} is negative, we can reduce the hole sizes starting from the outermost tapered holes. An alternative way is to choose a resonator with fewer tapered holes, such as the resonators with $n_t = 4$ designed in Section 3.

Figures 8(a) and 8(b) show the spectra of transmission and group delay of an $N = 10$ Butterworth CROW and an $N = 10$ Bessel CROW, respectively. The values of transmission at the band center are both 0.916, indicating a small intrinsic loss due to the large group delay in addition to the scattering loss at the input. Substracting the scattering loss which corresponds to a transmission of 0.955, the intrinsic Q can be obtained from the intrinsic loss and the group

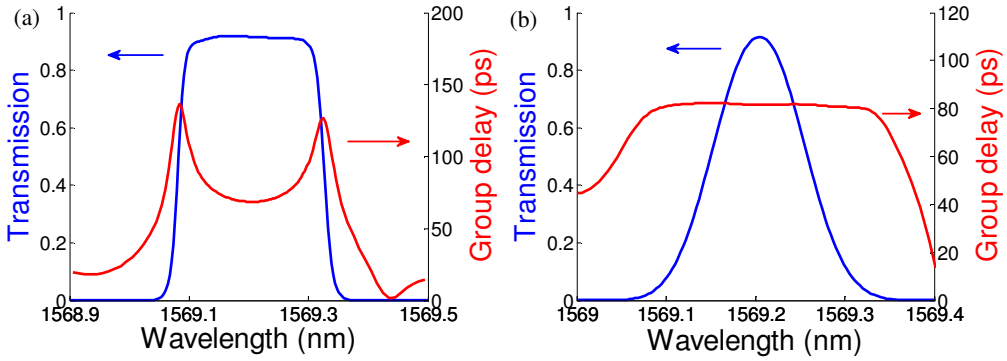

Fig. 8. Spectra of transmission and group delay of (a) an $N = 10$ Butterworth grating CROW and (b) an $N = 10$ Bessel grating CROW.

#161978 - $15.00 USD Received 7 Feb 2012; revised 30 Mar 2012; accepted 2 Apr 2012; published 6 Apr 2012

delay and is determined to be 2.34×10^6 and 1.97×10^6 for Butterworth and Bessel CROWs, respectively. Therefore, the tailoring of coupling coefficients does not degrade the Q of the resonators. In practice, the Q of the resonators may degrade due to imperfection of fabrication. With larger intrinsic loss, the transmission spectrum of Butterworth CROWs may be distorted since the loss is proportional to the group delay. A predistortion technique can be applied to pre-compensate for the distortion provided that the Q can be estimated and is uniform over the CROW [18]. Since the group delay of Bessel CROWs is flat within the bandwidth, the transmission spectrum is not distorted by uniform resonator loss.

6. Effect of fabrication disorder on grating-defect CROWs

The major limitation in the experiment of CROWs has been the unavoidable fabrication imperfection which leads to disorder in the resonant frequency of each resonator and the coupling coefficients. The disorder distorts the CROW response and limits the minimum bandwidth which CROWs can be designed with. The yield of CROWs drops as the number of resonators is increased or as the CROW bandwidth is decreased. The effect of disorder on CROWs has been investigated in the literature [21, 22]. In this section we analyze the disorder effect on grating-defect CROWs.

Due to the ultra-small modal volume of the grating-defect resonators designed in this paper, the shift of resonant wavelength due to deviation of hole radii is relatively large. Figure 9(a) shows the wavelength shift corresponding to 1 nm change of radius for each hole starting from the one nearest to the defect. Since the mode is concentrated near the defect, the resonant wavelength is more sensitive to the deviation of the first three holes. If the standard deviation of each hole radius is δr = 1 nm, the standard deviation of the resonant wavelength, considering holes on both sides of the defect, is $\delta\lambda$ = 0.8 nm. Depending on the fabrication quality (δr), the minimum CROW bandwidth is limited by $\delta\lambda = 0.8 \cdot \delta r$. Figures 9(b) and 9(c) show the simulated transmission spectra of 10-resonator CROWs with uniform coupling coefficient in the presence of disorder in resonant frequency, $\delta\omega$. The CROW bandwidth is 2B, and $\delta\omega$ are 0.5B and 0.25B respectively. The disorder leads to oscillations in the passband. Considering the center half of the bandwidth, the averaged oscillation amplitudes are 12.0 dB and 4.0 dB, respectively. The disorder of coupling coefficient is relatively small.

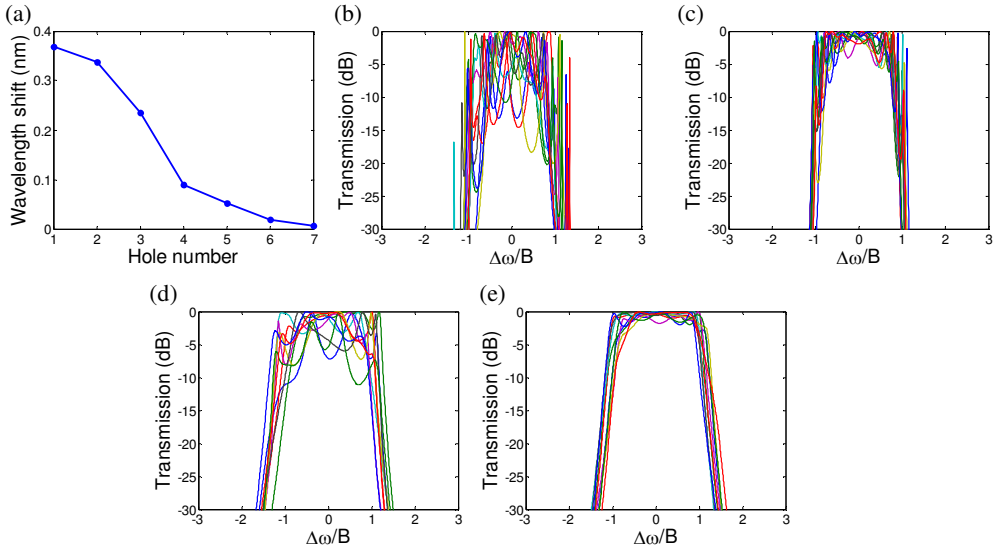

Fig. 9. (a) Shift of resonant wavelength due to 1 nm change of radius for each hole starting from the one nearest to the defect. (b-e) Simulated transmission spectra of 10-resonator CROWs with disorder in resonant frequencies. (b,c) Uniform coupling coefficients. (d,e) Butterworth filters. (b,d) $\delta\omega$ = 0.5B. (c,e) $\delta\omega$ = 0.25B.

#161978 - $15.00 USD Received 7 Feb 2012; revised 30 Mar 2012; accepted 2 Apr 2012; published 6 Apr 2012

For δr = 1 nm, $\delta\kappa/\kappa$ = 3%. For the bandwidth of interest, the distortion due to $\delta\kappa$ is negligible compared to the distortion due to $\delta\omega$.

The oscillations in the passband can be reduced by applying Butterworth filter design. Figures 9(d) and 9(e) show the simulated spectra of Butterworth CROWs with the same bandwidth and the same $\delta\omega$ as in Figs. 9(b) and 9(c). The average oscillation amplitudes are reduced to 4.4 dB and 1.1 dB, respectively. The disorder is a perturbation to an ideal CROW and can be taken as scatterers in the CROW. For CROWs with uniform coupling coefficient, the boundaries between the CROW and the waveguides cause reflection and form a cavity. Disorder in uniform CROWs can be thought of as scatterers in a cavity which can cause large oscillations. In a Butterworth CROW, the coupling coefficients are tailored to adiabatically transform between the CROW and the waveguides, thereby removing the cavity and reducing the amplitude of oscillations.

Because of the higher wavelength sensitivity of grating-defect resonators compared to those of larger resonators such as ring resonators, grating-defect CROWs designed in this paper are more practical for larger bandwidth applications (for example, in our experimental results [23], 1, 3, and 10 nm). Although larger bandwidth corresponds to smaller delay, the group velocity is still small considering the length of grating-defect resonators. If the grating is chosen to be weaker, such as shallower holes, the wavelength sensitivity will become smaller due to the larger modal size. Therefore, the length of each resonator and the wavelength sensitivity appear to a trade-off in the design of grating-defect CROWs.

7. Conclusion

We have demonstrated a systematic approach to design high-Q tapered grating-defect resonators, control the inter-resonator coupling, and design high-order grating CROW filters. The formalism based on coupled-mode theory is valid in strong gratings, with the help of 3D simulations for the characterization of gratings. The optimized Q of 2.16×10^6 is an order of magnitude higher than the theoretical Q of grating-defect resonators designed in the literature. Based on these high-Q resonators, CROWs which are shorter than 60 μm exhibit a group delay of more than 100 ps while maintaining a transmission of 0.9. The control of inter-resonator coupling via the number of holes provides a convenient way of designing coupled-resonator structures. Furthermore, we demonstrated the design of tenth-order Butterworth and Bessel filters which possess maximally flat transmission and group delay, respectively. Besides flat transmission, Butterworth CROWs are more robust against fabrication disorder compared to CROWs with uniform coupling coefficient.

The grating-defect CROWs designed in this paper are attractive for their small footprints, high quality factors, and their natural coupling to input and output waveguides. The coupled-mode formalism developed in this work can be further applied to other types of strong grating structures to minimize the coupling to radiation modes and reliably calculate the transfer function of grating structures when the coupling to radiation modes is negligible.

Appendix. Inline coupling of resonators

Inline resonators are, by definition, fabricated, cascaded, and coupled in a single waveguide. The objective of this appendix is to derive the inter-resonator coupling coefficient as a function of individual quality factors and the length of the coupling waveguide.

Figure 10(a) shows a symmetric inline resonator, i.e. the coupling to the waveguides is equally strong on both sides. In a symmetric grating-defect resonator, the number of holes on both sides of the defect is equal. The time-domain coupled-mode equations of the structure in Fig. 10(a) are

#161978 - $15.00 USD Received 7 Feb 2012; revised 30 Mar 2012; accepted 2 Apr 2012; published 6 Apr 2012

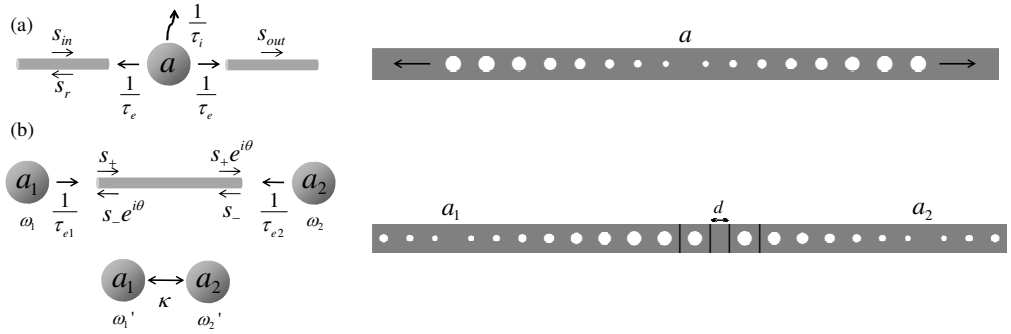

Fig. 10. Schematic drawings and the corresponding grating structures of (a) a symmetric resonator and (b) inline coupling of two resonators.

$$\begin{aligned} \frac{da}{dt} &= (i\omega - \frac{1}{\tau_i} - \frac{2}{\tau_e})a - i\mu s_{in} \\ s_{out} &= -i\mu a \\ s_r &= s_{in} - i\mu a \end{aligned} \quad , \tag{13}$$

where a is the resonator mode amplitude, s_{in}, s_r, and s_{out} are the input, reflected, and transmitted mode amplitudes respectively, ω is the resonant frequency, $1/\tau_i$ and $1/\tau_e$ are the intrinsic loss and the external loss to each waveguide respectively, and μ is the waveguide-resonator coupling. It can be shown that $\mu = \sqrt{2/\tau_e}$ using conservation of energy. The quality factor of the resonator is given by $Q = \omega\tau/2$, where $1/\tau = 1/\tau_i + 2/\tau_e$ is the total loss rate. In the regime where intrinsic loss is negligible (the linear region in Fig. 5(d)), $Q = \omega\tau_e/4$. Therefore, we obtain $1/\tau_e = \omega/(4Q)$ if Q is given.

In Fig. 10(b), we consider two inline resonators cascaded in a waveguide. The inter-resonator coupling is via the coupling waveguide of length d. The coupled-mode equations of the two resonators and the coupling waveguide are given by

$$\begin{aligned} \frac{da_1}{dt} &= (i\omega_1 - \frac{1}{\tau_{e1}})a_1 - i\mu_1 s_- e^{i\theta} \\ \frac{da_2}{dt} &= (i\omega_2 - \frac{1}{\tau_{e2}})a_2 - i\mu_2 s_+ e^{i\theta} \\ s_+ &= s_- e^{i\theta} - i\mu_1 a_1 \\ s_- &= s_+ e^{i\theta} - i\mu_2 a_2 \end{aligned} \quad . \tag{14}$$

The notations are shown in Fig. 10(b). θ is the phase accumulated in the propagation. The resonant frequencies and the external losses of the two resonators can be different in general. The intrinsic losses and the coupling to the other resonators or waveguides have been ignored and can be added to the equations. Combining the last two equations of Eq. (14), s_+ and s_- can be expressed as linear combinations of a_1 and a_2, and Eq. (14) can be rewritten as coupled-mode equations of two directly coupled resonators (also shown in Fig. 10(b)):

$$\begin{aligned} \frac{da_1}{dt} &= i(\omega_1 - \frac{\cot\theta}{\tau_{e1}})a_1 - i\frac{\csc\theta}{\sqrt{\tau_{e1}\tau_{e2}}}a_2 \\ \frac{da_2}{dt} &= i(\omega_2 - \frac{\cot\theta}{\tau_{e2}})a_2 - i\frac{\csc\theta}{\sqrt{\tau_{e1}\tau_{e2}}}a_1 \end{aligned} \quad . \tag{15}$$

#161978 - $15.00 USD Received 7 Feb 2012; revised 30 Mar 2012; accepted 2 Apr 2012; published 6 Apr 2012

The coupling leads to detuning of resonant frequencies and a coupling coefficient which depend on the round-trip phase of the coupling waveguide cavity, 2θ:

$$\begin{aligned} \Delta\omega_{1,2} &= -\frac{\cot\theta}{\tau_{e1,2}} \\ \kappa &= \frac{\csc\theta}{\sqrt{\tau_{e1}\tau_{e2}}} \end{aligned}. \tag{16}$$

When designing CROWs, we require identical resonant frequencies. If the frequency detuning $\Delta\omega$ is nonzero, the resonators in a CROW may experience different frequency detuning. For example, the frequencies of the first and last resonators are less detuned since they only couple to one resonator, while the other resonators have two neighbors. Therefore, we require $\Delta\omega = 0$, which corresponds to $2\theta = \pi$, a totally destructive interference in the coupling cavity. $2\theta = \pi$ also leads to a minimal coupling coefficient. The cavity round-trip phase includes the phase of reflection from the grating and the propagation phase in the cavity. At the Bragg wavelength, the reflection phase $\theta_r = -\pi/2 - \sin^{-1}(\delta/\kappa_g)$ is $-\pi/2$. Therefore, the round-trip phase with $d = 0$ is already π. This is an important reason why we choose to work at the Bragg wavelength. If the resonance is near the band edge, an additional coupling waveguide of length d is required to satisfy a round-trip phase of π [24]. The coupling coefficient for the grating-defect resonators in this paper is thus given by

$$\kappa = \frac{1}{\sqrt{\tau_{e1}\tau_{e2}}} = \frac{\omega}{4\sqrt{Q_1 Q_2}}, \tag{17}$$

which proves Eq. (7).

Acknowledgments

The authors thank Christos Santis for helpful discussions. This work was supported by National Science Foundation and The Army Research Office.

#161978 - $15.00 USD Received 7 Feb 2012; revised 30 Mar 2012; accepted 2 Apr 2012; published 6 Apr 2012